We wish to thank the reviewers for their insightful comments, which substantially improved the revision. In this response to reviewers we have focused only on comments that led to revisions. For the fuller discussion that includes our responses to all reviewer points, please see the reply we published in December.

The major changes we made to the manuscript in this revision are: 1) we performed CFD model calculations over the actual topography from one of our study sites to demonstrate that the model reproduces the measured z0 value, 2) we demonstrated the multi-scale control on z0 by filtering the topography to show that a different z0 value is obtained when high-wavenumber variability is removed, and 3) we developed a simple predictive equation for z0 that does not rely on using the Fourier transform. This alternative equation (denoted equation (5) in the revised paper) does not work as well as the Fourier transform approach but it comes close. As such, both equations have their place (equation (4) is more accurate but equation (5) is simpler to apply).

Reviewer 1:
Q: "*3. The CFD parameters are presented in a dimensional way, which is problematic. Rather than lengths and velocities, Reynolds numbers are relevant, and ratios, e.g. z_0g, height, and amplitude of the sinusoid in comparison to the viscous depth nu/u_*. Also I don't understand why the authors do not use periodic boundary conditions, in order to avoid an undesired fetch effect. How is modelled the micro-scale roughness z_0g in the k-epsilon code?*"
A: Reynolds numbers are relevant, but the reader has been provided all of the information to calculate them. We don't think that all CFD model studies must present results in dimensionless form. The height of the viscous sublayer is approximately 0.4 mm at threshold, decreasing to smaller values with increasing u* (Kok et al., 2012). Therefore, the viscous sublayer is much smaller than the roughness elements assumed in our CFD models. The micro-scale roughness is included in the model as a boundary condition on the gradient of the turbulent flow velocity (if turbulence is present) within the cells nearest the ground. Flow within these cells is assumed to be logarithmic in form with micro-scale roughness length z0g if the flow is turbulent, otherwise a laminar profile is used based on the viscosity of air. We have not experimented with periodic boundary conditions in the PHOENICS CFD model but will pursue this in the future – thanks to the reviewer for this excellent suggestion. We propose to add the following sentence to section 2.3: "In the CFD model the ground surface is treated using a wall-function approach, i.e. the velocity profile within the first cell is assumed to be logarithmic with a microscale roughness length equal to z0g if the flow is turbulent, otherwise a laminar profile is used based on the viscosity of air."

Q: "*4. The authors should give a precise definition of what they call the 'roughness sublayer'. Is it the same as what is usually called the viscous sublayer, of thickness nu/u_*, where the wind profile is not logarithmic, as described by e.g. van Driest (1956)?*"
A: The viscous sublayer and the roughness sublayer are not the same. Both are regions where mixing-length theory breaks down, but in the first case it is because flow is laminar and in the second case because the structure of the flow is strongly influenced (e.g. via flow separation) by individual roughness elements of the surface.
        The roughness sublayer is a fairly well-known aspect of rough boundary layer flows and is defined by the American Meteorological Society (http://glossary.ametsoc.org/wiki/Roughness_sublayer) as "The lowest atmospheric layer

immediately adjacent to a surface covered with relatively large roughness elements such as stones, vegetation, trees, or buildings. The roughness sublayer extends from the surface up to about two to five times the height of the roughness elements. Within the roughness sublayer the flow is three-dimensional, since it is dynamically influenced by length scales of individual roughness elements and surface layer scaling cannot be expected to apply". In the discussion paper we defined the roughness sublayer as "the range of heights above the ground comparable to the height of the largest roughness elements." In the revised manuscript we propose to include the following two sentences to clarify this issue: "The roughness sublayer is the layer where the mean velocity profile deviates from the law of the wall as the flow interacts with individual roughness elements. This layer is typically considered to extend from the ground surface to a height of approximately twice the height of the tallest roughness elements."

Q: "*5. Fitting z_0: Adjusting a log-profile on the direct data, or fitting a straight line on the log of the data is not equivalent, and the later gives more weight on the data close to the surface. What was the choice of the authors? How were error bars in velocity measurements (or data dispersion due to fluctuations) accounted for in the fitting process?*"
A: Our procedure for fitting the data was described on p. 1116, i.e. "least-squares fitting of the wind velocities to the natural logarithm of the distance above the ground. The shear velocity is equal to the slope of u vs. ln z multiplied by kappa. The roughness length is equal to the exponential of the following: minus the intercept divided by the slope." This procedure precisely follows Bergeron and Abrahams (1992), equations (6) and (7). We propose to add the following sentences to the revised paper to clarify this issue: "To extract a z_0 value from the velocity profile data, we followed the procedure of Bergeron and Abrahams (1992), who emphasized the need to regress *u* on ln *z* rather than ln *z* on *u*. The shear velocity is equal to the slope of the regression of *u* on ln *z* multiplied by kappa (equation (6) of Bergeron and Abrahams (1992)) and the roughness length is equal to the exponential of the following: minus the intercept divided by the slope (equation (7) of Bergeron and Abrahams (1992))."

Q: "*6. A few missing references that could be relevant: Taylor et al., Boundary-Layer Met. 1989 Raupach et al., Appl. Mech. Rev. 1991 van Rijn, J. Hydraul. Div. 1983.*"
A: The first reference was added to the revised paper in the introduction. We did not think it necessary to cite the Raupach et al. 1991 paper since we are already citing two Raupach papers of the same vintage that are more directly relevant to our topic. We could not find van Rijn, J. Hydraul. Div. 1983. When we went to this authors list of publications (http://www.leovanrijn-sediment.com/) and looked under "1. Bed forms and bed roughness", there was no paper from 1983.

Q: "*7. Error bars are missing in Fig. 6.*"
A: The sensor accuracy as reported by the manufacturer is 0.2 m/s. As this error is independent of wind speed, it is not necessary to weigh the measurements in the regression. It is difficult to provide error bars on Fig. 6, however, since the error for a 12-s average value may be lower than 0.2 m/s due to averaging 12 1-s measurements. We have almost never seen error bars plotted on wind velocity profiles for this reason. There is certainly variability in wind speed computed within each 12 s interval, but the literature indicates that one should not attempt to measure a mean velocity for the purposes of estimating mean velocity profiles using any time interval less than approximately 10 s (e.g. Namikas et al., 2003), as discussed in the paper.

Q: "*8. As the authors discuss, I have a problem with a Fourier analysis of a non-linear problem, and to me it would make more sense to extract a relevant length (for a given problem) from the Fourier spectrum of the bed elevation, and apply a formula like (3), rather than summing up over the whole spectrum like in (4).*"

A: We have developed an alternative equation (equation (5)) that is simpler. Here is the new text in the Methods section:

"An alternative approach to equation (4) that is easier to apply and does not rely on the Fourier transform is

$$z_0 = z_{0g} + c_5 H_{\text{RMSE}} S_{\text{av}}^{c_6} . \tag{5}$$

where c_5 and c_6 are unitless coefficients.

And in the Results section:

"An alternative approach is to use the values of H_{RMSE} and S_{av} to estimate z_0 using equation (5). We found $c_5 = 16$ and $c_6 = 2.0$ to yield the highest R^2 value (0.978). Equation (5) is thus a useful formula with an advantage of simplicity, but it is somewhat inferior to the multi-scale analysis of equation (4) based on its lower R^2 value."

In the discussion we have also addressed this issue as follows:

"The CFD model results demonstrate that equation (3) works well for a single sinusoid, while equation (4) works well for real-world cases that can be represented as a superposition of many (i.e., $N \gg 1$) sinusoids. The fact that the value of c_4 is larger than c_1 indicates that there is no seamless transition between equation (3) and equation (4) as the topography changes from the idealized case of a single sinusoid to the case of many superposed sinusoids. That is, neither formula works well for the case of a small number of superposed sinusoids. The absence of such a seamless transition could be a result of applying the superposition principle to a nonlinear problem (boundary layer turbulence) for which it cannot apply precisely. In addition, experimental studies demonstrate that flow separation (which influences z_0) is a function of both the slope and the curvature of the bed (Simpson, 1989; Lamballais et al., 2010). Equations (3) and (4) do not utilize curvature, hence neither equation can be the basis of a perfect method for predicting z_0. It is likely that the only way to precisely estimate z_0 is to compute the actual flow field over the topography using a CFD model. Any other approach will likely involve some type of approximation. We propose that equation (4), while imperfect, yields a good approximation for z_0 values in real-world terrain (i.e. those with many Fourier coefficients contributing to z_0), based on the R^2 value of 0.991 we obtained. Equation (5) provides an alternative for users who prefer its simplicity. Equation (5) is not accurate for all possible S_{av} values, since z_0 cannot increase without bound as S_{av} increases. As such, equation (5) should only be considered applicable to microtopography with S_{av} values less than approximately 0.15."

Reviewer 2:
Q: "*1- Multi-scale analysis: There is no evidence in the paper that the fact a topography has multiple scales affects the roughness length in any meaningful way. The CFD simulations are run with single scale sinusoidal surfaces, while there is no clear way to measure the contribution to the roughness length from the different scales within the topography. I suggest the authors to use the CFD code to test this hypothesis and run simulations with multi-scale synthetic data (with few sinusoidal modes to get a better picture). That way they could compare the simulations with predictions using either Eq. 3 with an effective amplitude and slope or Eq.*

4. Without this basic information any discussion of the effect of multiples scales is merely speculative."

A: If one accepts that both the amplitude and slope of microtopographic variations influence the effective roughness length (which we showed in Figure 10 for the case of a sinusoid), it follows that there is no single Fourier mode that controls the effective roughness length, unless the topography is a perfect sinusoid (which it never is). This is because the slope is a high-pass filter of the topography (i.e. the slope is proportional to $k*a_n$ where a_n is the Fourier coefficient) and hence is more sensitive to high-wavenumber components of the topography than the amplitude is.

However, it is straightforward to demonstrate using the CFD model that the effective roughness length is a function of the multi-scale variability of the microtopography. In the revision we used one of the playa profiles (we chose the Soda Lake smooth site but similar results are obtained for other profiles) to compute the effective roughness length with and without smoothing of the topography (see text below). This analysis shows that the effective roughness length decreases as the high-wavenumber variations are removed, i.e. that the roughness length depends on the microtopography at multiple scales.

We disagree with the reviewer's contention that there is "no clear way to measure the contribution to the roughness length from the different scales within the topography." This is precisely what Figure 11 shows, i.e. how different scales within the topography contribute to z0. New text and figures we propose to add:

"To demonstrate the suitability of PHOENICS for modeling atmospheric boundary-layer flows and to establish that the effective roughness length depends on the microtopographic variability at multiple scales, we performed a numerical experiment using the central microtopographic profile measured at the Soda Lake smooth site as input (plotted in Fig. 9A). We measured a mean z_0 value of 4.6 mm from velocity profiles at this site. Figure 9B presents the velocity profiles predicted by the PHOENICS model for 2D flow over the profile, following the procedures detailed in the Methods section. PHOENICS predicts an effective roughness length of 2.4 mm based on a least-squares fit of the velocity to the logarithms of distance above the ground from a height equal to twice the height of the dominant roughness elements to the top of the model domain. As such, the PHOENICS model predicts a z_0 value similar to the value we measured in the field (relative to the four order-of-magnitude variation in z_0 values we measured across the study sites).

To demonstrate that the z_0 value depends on microtopographic variability at multiple scales, we filtered the Soda Lake smooth profile diffusively to remove some of the small-scale (high-wavenumber) variability while maintaining the large-scale variability (i.e. the root-mean-squared variability of the filtered and unfiltered profiles is identical). Figure 9 plots the original profile, the filtered profile, and their amplitude and z_{0n} spectra. The z_0 values for the unfiltered and filtered cases are 2.4 mm and 0.15 mm, respectively, based on fitting the velocity profiles predicted by PHOENICS. That is, the filtered profile has a z_0 value more than an order of magnitude smaller than the original profile despite the fact that the amplitude of the large-scale microtopographic variations is the same as the original profile. Equation (4) predicts 2.8 mm and 0.25 mm, respectively, for the z_0 values. The z_0 value decreases in the filtered case because steep slopes that trigger flow separation are significantly reduced at a wide range of scales by filtering, lowering the z_0 value.

The results of this numerical experiment demonstrate that z_0 values depend on variability microtopographic variability at multiple scales. There is also a general theoretical argument that

supports this conclusion. If one accepts that both the amplitude and slope of the microtopography influence the effective roughness length (which we demonstrate below for the case of a single sinusoid), it follows that there is no single Fourier mode that controls the effective roughness length, unless the topography is a perfect sinusoid. This is because the slope is a high-pass filter of the topography (i.e. the slope is proportional to $k*a_n$ where a_n is the Fourier coefficient) and hence is more sensitive to high-wavenumber components of the topography than the amplitude is."
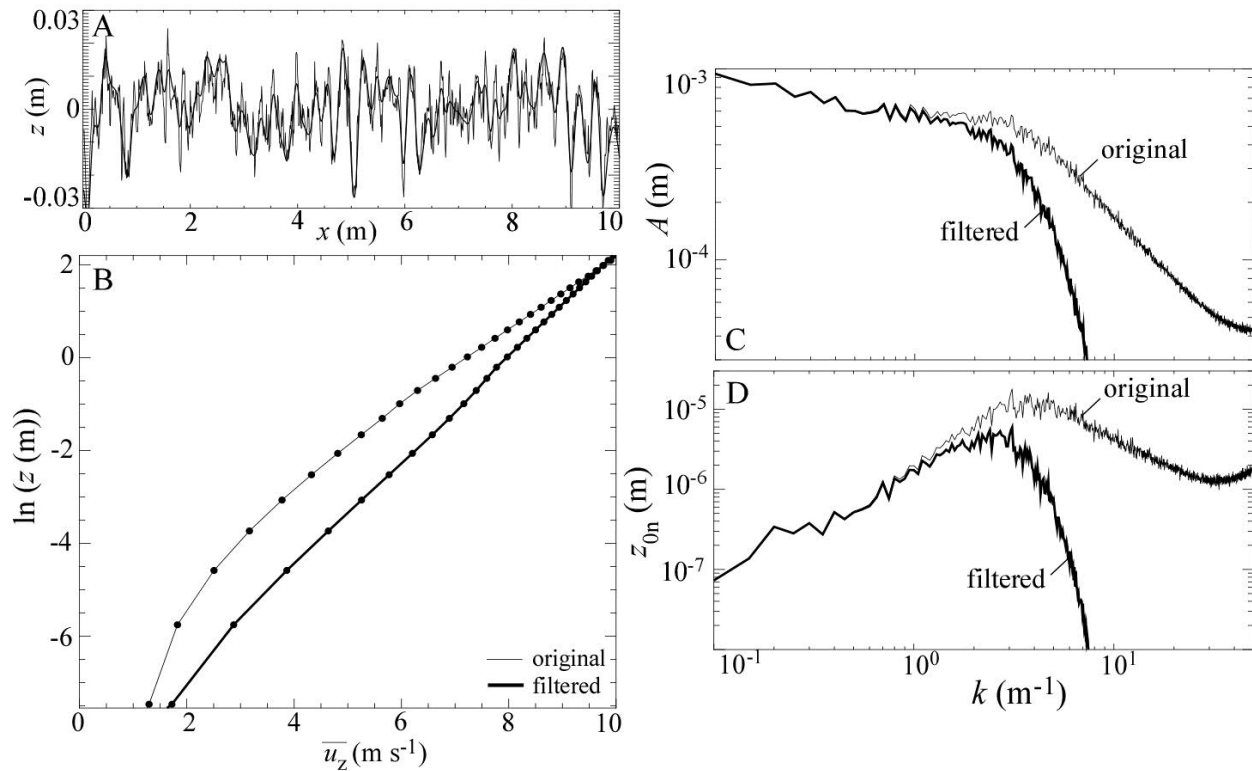

Figure 9. Demonstration of the dependence of z_0 values on the multi-scale nature of microtopography. (A) Plot of a profile through the Soda Lake smooth site (thin curve). Also shown is the same plot with diffusive smoothing (thicker curve). Smoothing maintains the amplitude of microtopographic variations at large spatial scales (i.e. the amplitude spectrum is unchanged at large scales) but removes some of the small-scale (high-wavenumber) variability. (B) Plots of the mean velocity profiles predicted by PHOENICS over the original and filtered profile. (C) Amplitude spectra of the two plots in (A). (D) Contributions of each Fourier mode to the z_0 values for the two plots in (A).

Q: "*3- Validation of the CFD model: It is not clear to me that the CFD code is actually able to reproduce the real trends of the measured roughness length on different surfaces. Why not use the measured microtopography to run the model and compare? Even a qualitative comparison will strengthen the argument of the CFD model as a tool to develop expressions for the roughness length.*"
A: The PHOENICS model has been the source of many CFD studies of atmospheric boundary layer flows since its original formulation c. 1974. PHOENICS is the engine of WindSim, which is a leading code for boundary-layer flow modeling in wind engineering applications. As such, the model has been successfully used for atmospheric flows for over 40 years.

That said, it is straightforward to include the results of CFD model runs over one of our actual surface profiles to demonstrate that it predicts a similar roughness length to that we measured. See Figure 9 and associated text above.

Q: "*End of page 1121: The description of Fig. 6 is wrong, a steeper slope doesn't necessarily correspond to a smaller z_0. Please correct with the new version of Fig. 6 (see above).*"

A: A steeper slope does necessarily correspond to a smaller intercept (and hence z0) when the velocity data are normalized as in Figure 6. To see this, consider the equation for a line: y = mx+b. If the values of y are normalized such that y(x0) = 1, where x0 is a constant, it follows that the slope of the line, m, is equal to $(1-b)/x0$. That is, a steeper slope necessarily corresponds to a smaller intercept (hence z0) value.

We agree that the two sentences on p. 1121, lines 22-23, are not precisely correct as written. We wrote "The law of the wall predicts a constant slope when u is plotted vs. ln z. A steeper slope corresponds to a smaller z0 value." We should have made clear that the plots of u vs. ln z we were referring to were those normalized as in Fig. 6. In the revision we propose to write "The law of the wall predicts a constant slope when u is plotted vs. ln z. When the velocities are normalized as in Figure 6, a steeper slope corresponds to a smaller z0 value."

Jon Pelletier

All changes in red:

Predicting the roughness length of turbulent flows over landscapes with multi-scale microtopography

Jon D. Pelletier[*] and Jason P. Field

Department of Geosciences, University of Arizona, Gould-Simpson Building, 1040 East Fourth Street, Tucson, Arizona 85721-0077, USA

*corresponding author; email: jdpellet@email.arizona.edu

Abstract

The fully rough form of the law of the wall is commonly used to quantify velocity profiles and associated bed shear stresses in fluvial, aeolian, and coastal environments. A key

parameter in this law is the roughness length, z_0. Here we propose a predictive formula for z_0 that uses the amplitude and slope of each wavelength of microtopography within a discrete-Fourier-transform-based approach. Computational fluid dynamics (CFD) modeling is used to quantify the effective z_0 value of sinusoidal microtopography as a function of the amplitude and slope. The effective z_0 value of landscapes with multi-scale roughness is then given by the sum of contributions from each Fourier mode of the microtopography. Predictions of the equation are tested against z_0 values measured in ~10^5 wind velocity profiles from southwestern U.S. playa surfaces. Our equation is capable of predicting z_0 values to 50% accuracy, on average, across a four order-of-magnitude range. We also use our results to provide a simpler alternative formula that, while somewhat less accurate than the one obtained from a full multi-scale analysis, has an advantage of being simple and easier to apply.

Keywords: boundary layer flow, law of the wall, roughness length, terrestrial laser scanning, computational fluid dynamics (CFD)

1. Introduction

1.1. Problem statement

The velocity profiles of turbulent boundary-layer flows are often quantified using the fully rough form of the law of the wall:

$$u(z) = \frac{u_*}{\kappa} \ln\left(\frac{z}{z_0}\right). \tag{1}$$

where $u(z)$ is the wind velocity (averaged over some time interval) at a height z above the bed, u_* is the shear velocity, κ is the von Kármán constant (0.41), and z_0 is an effective roughness length that includes the effects of grain-scale roughness and microtopography (e.g. Bauer et al., 1992; Dong et al., 2001). Velocity profiles measured in the field are commonly fit to equation (1) to

estimate u_* and/or τ_b for input into empirical sediment transport models (often after a decomposition of the bed shear stress into skin and form drag components) (e.g. Gomez and Church, 1989; Nakato, 1990). Fits of wind-velocity profiles to equation (1) also provide measurements of z_0. Given a value for z_0, a time series of u_* and/or τ_b can be calculated from equation (1) using measurements of velocity from just a single height above the ground. This approach is widely used because flow velocity data are often limited to a single height. Equation (1) only applies to $z \geq z_0$, and may be further limited in its accuracy within the roughness sublayer, i.e. the range of heights above the ground comparable to the height of the largest roughness elements. The roughness sublayer is the layer where the mean velocity profile deviates from the law of the wall as the flow interacts with individual roughness elements. This layer is typically considered to extend from the ground surface to a height of approximately twice the height of the tallest roughness elements. Values of z_0 depend on microtopography/land cover (quantifying this dependence in unvegetated landscapes is a key goal of this paper) and are typically in the range of 10^{-2}-10^{1} mm for wind flow over arid regions (Prigent et al., 2005).

Most existing methods for estimating z_0 using metrics of surface roughness or microtopography rely on the concept of a dominant roughness element, the size and density of which the user must specify *a priori* (e.g. Lettau, 1969; Arya, 1975; Smith and McLean, 1977; Jacobs, 1989; Taylor et al., 1989; Raupach, 1991,1992; 1994; Kean and Smith, 2006a). Procedures are available for estimating z_0 in landscapes with multi-scale roughness, but they often rely on idealizations such as treating the microtopography as a sequence of Gaussian bumps (e.g. Kean and Smith, 2006b). Nearly all natural landscapes have microtopographic variability over a wide range of spatial scales. Identifying the dominant scale objectively and uniquely can be difficult. For example, the top plot in Figure 1 shows a hypothetical case of a

landscape composed of two superposed sine waves. The effective roughness length of a landscape is related to the presence/absence or extent of flow separation, and flow separation is primarily controlled by the derivatives of topography (slope and curvature) rather than the amplitude of the bedforms/roughness elements (Simpson, 1989; Lamballais et al., 2010). As such, roughness elements of smaller amplitude but steeper slopes may exert greater control on z_0 values compared with roughness elements that are larger in amplitude but gentler in slope. Given a landscape with multi-scale roughness in which each scale has distinct amplitudes and slopes, it can be difficult to identify the dominant scale or scales of roughness for the purposes of estimating z_0.

Figure 1 illustrates two examples of microtopography from playa surfaces in the southwestern U.S. The middle plot shows a transect through the Devil's Golf Course in Death Valley, California and the bottom plot shows a transect through a relatively smooth section of Lordsburg Playa, New Mexico. These plots are presented using different vertical scales because the amplitude of the microtopography at the Death Valley site is approximately 100 times greater than that of the Lordsburg Playa site. Both landscapes have no vegetation cover, no loose sand available for transport, and are flat or locally planar at scales larger than ~1 m. As such, they are among the simplest possible natural landscapes in terms of their roughness characteristics. Nevertheless, as Figure 1 demonstrates, they are characterized by significant roughness over all spatial scales from the resolution of the data (1 cm) up to spatial scales of ~1 m. To our knowledge, there is no procedure for predicting z_0 in a way that honors the multi-scale nature of microtopography in real cases such as these. To meet this need, we have developed and tested a discrete-Fourier-transform-based approach to quantifying the effects of microtopographic

variations on z_0.values. The method simultaneously provides an objective measure of the spatial scales of microtopography/roughness that most strongly control z_0.

In a recent paper similar in spirit to this one, Nield et al. (2014) quantified the z_0 values of wind velocity profiles over playas as a function of various microtopographic metrics. Nield et al. (2014) proposed an empirical, power-law relationship between z_0 and the root-mean-squared variations of microtopography, H_{RMSE}:

$$z_0 = cH_{RMSE}^{1.66} \tag{2}$$

where the coefficient c is equal to ln(-1.43) or 0.239 m$^{-0.34}$. Equation (2) is one example of several predictive formulae that Nield et al. (2014) proposed for different surface types (equation (2) applies to surfaces with large roughness elements or that exhibit mixed homogenous patches of large and small roughness elements). Nield et al. (2014) concluded that "the spacing of morphological elements is far less powerful in explaining variations in z_0 than metrics based on surface roughness height." In this paper we build upon the results of Nield et al. (2014) to show that z_0 can be most accurately predicted using a combination of the amplitudes and slopes of microtopographic variations ~~measured at multiple scales using Fourier analysis~~.

The presence of multi-scale roughness in nearly all landscapes complicates attempts to quantify effective z_0 values for input into regional and global atmospheric and Earth-system models. In such models, topographic variations are resolved at scales larger than a single grid cell (10-100 km at present, but steadily decreasing through time as computational power increases) but the aerodynamic effects of topographic variations on wind velocity profiles at smaller scales are not resolved in these models and must be represented by an effective z_0 value (sometimes in combination with an additional parameter, the displacement height, which shifts the location of maximum shear stress to a location close to the top of the roughness sublayer

(Jackson, 1981)). Topographic variations at spatial scales below 10-100 km are typically on the order of tens to hundreds of meters. Currently available maps of z_0 values do not incorporate the aerodynamic effects of topography at such scales. For example, Prigent et al. (2005) developed a global map of z_0 in deserts by correlating radar-derived measurements of decimeter-scale roughness with z_0 values inferred from wind velocity profiles. This approach assumes that the dominant roughness elements that control the effective z_0 value over scales of 10-100 km occur at the decimeter scale captured by radar. It is possible that, in some landscapes, the roughness that controls z_0 occurs at scales that are larger or smaller than those measured by radar. Therefore, a procedure is needed that predicts z_0 values using data for topographic variations over a wide range of scales, including but not limited to decimeter scales. This study aims to fill that gap.

1.2. Study Sites

We collected wind-velocity profiles and high-resolution topographic data using terrestrial laser scanning (TLS) from ten playa sites in the southwestern U.S. (Fig. 2) during the spring of 2015. These sites were selected based on the range of microtopographic roughness they exhibit (Table 1). Roughness can be quantified in multiple ways, but H_{RMSE}, the root-mean-squared deviation of elevation values measured at a sampling interval of 0.01 m, provides one appropriate metric (Nield et al., 2014). The ten sites range in H_{RMSE} from approximately 0.55 mm to 36 mm (see Section 2.1). In addition to the H_{RMSE} we computed S_{av}, the average slope computed at 0.01 m scale, for each site. Values of S_{av} range from 0.01 to 0.159 (Table 1).

Each study site was an area of at least 30 m x 30 m with relatively uniform roughness, as judged visually and by analysis of the TLS data. The minimum fetch required for an equilibrium boundary layer flow is typically assumed to be 1000 times the height of the dominant roughness

elements (Counehan, 1971). Based on this criterion, 30 m was adequate fetch for seven of the ten sites, i.e. all except for the three Death Valley sites, where roughness elements were up to 300 mm, hence the area of homogeneous roughness was verified to a distance of only ~100 times the height of the dominant roughness elements. However, the required fetch must also depend on the maximum height above the ground where velocities are measured to compute a z_0 value locally, since any roughness transition triggers an internal boundary layer that grows indefinitely in height with increasing distance downwind of the transition. Using the Elliot (1958) formula for the height of the internal boundary layer downwind of a roughness transition, the minimum fetch required for an log-law profile between 0 and 3 m above the ground over a landscape with $z_0 \approx$ 30 mm (the value measured at the Death Valley rough site) is 31.8 m. According to this alternative criterion, 30 m may be adequate for an equilibrium boundary layer flow to be established to a height of 3 m despite the limited fetch-to-roughness height ratio at the Death Valley sites.

The playa surfaces at our study sites were predominantly crusted and ranged from flat, recently formed crust to well-formed polygons with deflated and broken crust ridges. All of the sites were completely devoid of vegetation. Sand blows episodically across some portions of the playas we studied but we chose study areas in which we observed no sediment transport during fast winds. We considered only landscapes without vegetation and loose, erodible sand because such cases must be understood first before the additional complications of flexible roughness elements and saltation-induced roughness can be tackled. That said, we anticipate that concepts from this paper may be relevant to quantifying z_0 over vegetated landscapes also.

Our goal is to understand the controls on boundary layer flows over rough terrain generally, not playa surfaces specifically or exclusively. As such, we use playa surfaces as

"model" landscapes. Playas are useful for this purpose because they are macroscopically flat but exhibit a wide range of microtopographic roughness at small scales. The relative flatness of playas at scales larger than ~1 m makes it possible to characterize their boundary layer flows using relatively short anemometer towers. Of course, playas are also of special interest to aeolian geomorphologists because they can be major dust sources when sand from playa margins is transported across the playa surface, disturbing crusted surfaces and liberating large volumes of silt- and clay-rich sediments.

The questions addressed in this paper could, in principle, be addressed using wind tunnel experiments. Wind tunnels certainly have the advantage of user control over wind velocities. However, Sherman and Farrell (2008) documented that z_0 values in wind tunnels are, on average, approximately an order of magnitude lower than those measured in the field for otherwise similar conditions (e.g. grain size). One interpretation of the Sherman and Farrell (2008) results is that the confined nature of wind tunnel flows and/or their limited fetch can limit the development of boundary layers in equilibrium with bed roughness. For this reason, we focused on measuring wind flow over natural surfaces with homogeneous roughness characteristics over distances of at least 30 m surrounding our measurement locations.

2. Methods

2.1. Terrestrial laser scanning and analyses of playa surface microtopography

A Leica C10 terrestrial laser scanner was used to acquire point clouds of the central 10 m x 10 m ground surface upwind of the anemometers at each of the 10 study sites. The areas surrounding each 10 m x 10 m area were also surveyed to check for approximate homogeneity in the roughness metrics out to areas of 30 m x 30 m, but the central 10 m x 10 m areas were the

focus of the subsequent data analysis. Each area was scanned from four stations surrounding the 10 m x 10 m area and merged into a single point cloud using a Leica disk target system. Registration errors were a maximum of 2 mm in all cases. The Leica C10 has an inherent surface-model accuracy of 2 mm, but this value decreases as the number of overlapping scans increases (Hodge, 2010), resulting in a value of approximately 1 mm in the case of four overlapping scans. The scanner was mounted on a 3.5 m tripod to maximize the angle of incidence (low angles of incidence elongate the "shadows" or occlusions behind microtopographic highs (Brown and Hugenholtz, 2013)). All of the returns within each 1 cm^2 domain were averaged to create a Digital Elevation Model (DEM) with point spacing of 0.01 m. Voids were filled using natural-neighbor interpolation. Voids requiring interpolation were limited to <1% of the area at the smoothest five sites (Lordsburg and Willcox Playas), between 1% and 3% at the two Soda Lake sites, and between 10% and 20% at the three Death Valley sites.

In addition to the calculation of basic topographic metrics such as H_{RMSE} and S_{av} (the latter being the average slope computed at 0.01 m scales) (Table 1), we also computed the average amplitude spectrum of all 1D topographic transects at each study site. The amplitude spectrum is equal to two times the absolute value of the complex discrete Fourier transform (DFT). The average amplitude spectrum refers to the fact that the one thousand amplitude spectra of each 1D transect computed along the east-west direction were averaged to obtain a single average spectrum for each study site. We used the DFT implemented in the IDL programming language. The DFT coefficients were also used as input to a filter that uses the amplitude and slope of each Fourier mode to compute its contribution to the z_0 value. We created "mirror" images of each transect before application of the DFT. This approach has been shown

to work as well or better than windowing for minimizing truncation error (i.e. incomplete sampling) in data sets characterized by the broadband/multi-scale variability characteristic of many environmental data series (Smigelski, 2013).

2.2. Measurement and analyses of wind profiles

Wind speeds were measured at 1 s intervals and at 7 heights above the surface (0.01 m, 0.035 m, 0.076 m, 0.16 m, 0.52 m, 1.22 m, and 2.80 m) using four Inspeed Vortex rotating cup anemometers and four AccuSense hotwire anemometers (F900 series) (the latter calibrated to work over the 0.15-10 m s^{-1} range of wind velocities) (Fig. 3). The hotwire sensors were secured to an L-shaped steel frame and placed above the surface such that the small opening in the sensor head was oriented as perpendicular to the wind direction as possible (Fig. 3). The 10 m s^{-1} range of the hotwire sensors was not a limiting factor because all of the hot-wire sensors were located close to the ground, i.e. within 0.16 m from the surface, where velocities were lower than 10 m s^{-1} during our deployments. We collected data at each of the ten sites for ten to thirty hours spanning multiple days, times of day, and a wide range of wind velocities.

The lowest cup and the highest hotwire anemometers were positioned at the same height (0.16 m) above the surface to standardize measurements between the two types of wind sensors. When positioned at the same height, the hotwire sensors measured wind speeds (based on the factory calibration) that were approximately 10% lower than the values obtained from the cup anemometers. We used the ratio of the wind velocities measured by the bottom cup anemometer to the wind velocities measured by the top hotwire sensor to standardize the hotwire measurements to the cup anemometer measurements in real time. This scaling-factor approach also serves a second purpose, which is to minimize the effects of wind-direction variability on the velocities measured by the hotwire sensors. The cup sensors measure wind speeds effectively

from nearly any direction, but the hotwire sensors are required to be oriented within 20° perpendicular to the wind for greatest accuracy. The hotwires were manually repositioned following large and sustained changes in wind direction, but short-duration changes may have resulted in oblique incidence angles with a bias towards lower velocities. Continually rescaling the velocities measured by the highest hotwire sensor to the lowest cup sensor mitigated this potential problem.

Scaled values from the bottom three (0.01 m, 0.035 m, and 0.076 m) hotwire sensors were combined with the four cup anemometers to calculate shear velocities, u_*, and aerodynamic roughness lengths, z_0, based on the average velocities measured in each 12-s interval via least-squares fitting of the wind velocities to the natural logarithm of the distance above the ground. To extract a z_0 value from the velocity profile data, we followed the procedure of Bergeron and Abrahams (1992), who emphasized the need to regress u on ln z rather than ln z on u. The shear velocity is equal to the ~~inverse of the~~ slope of ~~u vs.~~ the regression of u on ln z multiplied by κ~~.~~ (equation (6) of Bergeron and Abrahams (1992)) and the roughness length is equal to the exponential of the following: minus the intercept~~.~~ divided by the slope (equation (7) of Bergeron and Abrahams (1992)). The 12-s interval was chosen based on the results of Nimakas et al. (2003), who found that time intervals greater than 10 s resulted in the most accurate results, while those obtained from smaller averaging intervals were less reliable. Values of z_0 can be influenced by deviations from neutral stability. A common way to address this issue is to remove profiles from the analysis in which the velocity at a given height is below some threshold value (e.g. Nield et al., 2014). In this study we repeated our analysis using only those profiles with a wind velocity of at least 3 m s^{-1} at a height of 0.16 m. The mean and standard deviations of z_0

were nearly identical to those obtained using all of the data, likely reflecting the fact that we targeted time periods of fast winds for measurement.

During the data collection, the hotwire sensors were moved to approximately 25-50 random locations within each site. We moved the hotwire sensors to numerous locations within each site because wind velocities measured close to the ground are sensitive to the microtopography of the specific spot above which they are measured, i.e. the z_0 value measured on the stoss side of a microtopographic high tends to be smaller than the z_0 value measured on the lee due to the convergence/divergence of flow lines. Since our goal was to characterize the average or representative z_0 value over each surface, it is appropriate to move the hotwire sensors around the surface to ensure that the results are not specific to one location but instead represent a statistical "sample" of the flow above the surface at multiple locations. This approach is also consistent with how the CFD model output was analyzed (see Section 2.3).

Velocity profiles can deviate from equation (1) close to the ground over rough terrain. As such, it is important to identify which sensors, if any, are located within the roughness sublayer prior to computing u_* and z_0 values by fitting wind velocity data to equation (1). To do this, we plotted the average of all wind velocity measurements at each site as a function of ln z. The results (described in Section 3.2) show that the lowest two (hotwire) sensors (located 0.10 and 0.035 m above the ground) at the three Death Valley sites and the rough Soda Lake site deviated noticeably from equation (1). The fact that these sensors were within the roughness sublayer is consistent with the fact that the height of the largest roughness elements at these sites is greater than or comparable to 0.035 m (the height of the second lowest sensor). Data from the lowest sensor at the next four smoothest sites (i.e. smooth Soda Lake, the two Willcox Playa sites, and the rough Lordsburg Playa site) also deviate noticeably from equation (1). Data from these

sensors were not used in the calculation of u_* and z_0 at those sites. In addition, we verified in all cases that the removal of these sensors deemed to be within the roughness sublayer improved the mean correlation coefficients, R^2, at each site. Only profiles with R^2 values greater than 0.95 were retained.

2.3. Computational fluid dynamics

CFD modeling was used to quantify the effects of the amplitude and slope of sinusoidal microtopography on z_0. We used the 2013 version of the PHOENICS CFD model (Ludwig, 2011) to estimate the time-averaged wind velocities associated with neutrally stratified turbulent flow over sinusoidal topography with a range of amplitudes and slopes. PHOENICS uses a finite-volume scheme to solve simultaneously for the time-averaged pressure and flow velocity. PHOENICS solves the flow equations using the iterative SIMPLEST algorithm of Spalding (1980), which is a variant of the SIMPLE algorithm of Patankar and Spalding (1972). The solution was considered converged when the state variables changed by less than 0.001% from one iteration to the next. We used the renormalization group variant of the k-ε closure scheme first proposed by Yakhot and Orszag (1986) and later updated by Yakhot et al. (1992), which is widely used for sheared/separated boundary layer flows.

Inputs to our model runs include a topographic profile (in these cases, a sinusoid of a prescribed amplitude and maximum slope), a grain-scale roughness length, z_{0g} (set to be 0.003 mm for all runs), and a prescribed horizontal velocity at a reference height far from the bed ($u_r = 10$ m s^{-1} at $z_r = 10$ m was used for all of the model runs presented). The value of z_{0g} was chosen based on the measured value of z_0 at the two flattest sites (Lordsburg smooth and intermediate), both of which yield $z_0 = 0.\text{003}\text{002}$ mm as described in Section 3.2. This value is also consistent with the grain-scale roughness expected at a site with a median grain size of fine sand if the

Bagnold (1938) relation $z_{0g} = d_{50}/30$ is used. The ground surface is prescribed to be a fully rough boundary, i.e. one that results in a law of the wall velocity profile characterized by a roughness length equal to z_{0g} (0.003 mm) and a shear velocity equal to $\kappa u_r / \ln(z_r/z_{0g})$ (0.26 m s^{-1}) in the absence of topography. In the CFD model the ground surface is treated using a wall-function approach, i.e. the velocity profile within the first cell is assumed to be logarithmic with a microscale roughness length equal to z_{0g} if the flow is turbulent, otherwise a laminar profile is used based on the viscosity of air. At the upwind boundary of the model domain an "inlet" law of the wall velocity profile is prescribed with a roughness length equal to z_{0g}. At the downwind boundary (i.e. the "outlet") a fixed-pressure boundary condition is used.

The computational grids we used consisted of 2D terrain-following coordinate systems. Thirty logarithmically spaced grid points were used in the vertical direction, ranging from 0.1 mm to 10 m above the bed. We used 2000 grid points in the horizontal direction. The absolute size of the horizontal domain varied depending on the slope of the bedforms. That is, the topographic profile was identical for all of the runs (except for the fact that an amplitude of 0.05 m used for half of the runs and an amplitude of 0.1 m was used for the other half). Steeper slopes were obtained by decreasing the horizontal grid spacing or "compressing" the input topographic profile horizontally. The minimum length/fetch of the model domain was 30 m. Our analysis of the wind profiles output by the model was restricted to the last 20% of the model domain, i.e. the portion farthest downwind. This was necessary because the upwind boundary of the model is a roughness transition triggered by the interaction of the input velocity profile (characterized by roughness length z_{0g}) with the microtopography. This roughness transition generates an internal boundary layer that grows with distance from the upwind end of the domain. Within the internal boundary layer, the velocity profile is characterized by an effective roughness length z_0 set by the

amplitude and slope of the bedforms. To properly compute the value of z_0 based on velocity profiles from the top of the roughness sublayer to a height of 3 m, it is necessary to restrict the analysis of the wind profiles to the downwind end of a model domain that is at least 30 m in length as described in Section 1.2.

Model runs were performed using two different amplitudes (0.05 and 0.1 m) and a range of maximum slopes from 0.001 to 2.0. Each of the four hundred vertical velocity profiles of the last 20% of the model domain were fit to equation (1) from the top of the roughness sublayer (assumed to be equal to twice the maximum height of the bedforms) to a height of 3 m (to match the maximum height measured in the field). The four hundred z_0 values were then averaged to obtain an effective z_0 value for each value of the sinusoidal amplitude and slope. Values of z_0 were fit to the expression

$$z_0 = z_{0g} + \frac{c_1 a}{1 + (c_2/S)^{c_3}},\qquad(43)$$

where a is the amplitude (in units of m) of the sinusoid, S is the maximum slope (the slope at the point of inflection of the sinusoid in units of m/m), and c_1, c_2, and c_3 are unitless coefficients.

2.4. Fourier analysis of topography and a multi-scale approach to quantifying z_0

The results of the CFD modeling (described in Section 3.3) suggest that the slope and amplitude of microtopographic variations control z_0 values via the sigmoidal relation of equation (43). This result provides a basis for quantifying the multi-scale controls on z_0 within a discrete-Fourier-transform-based approach that treats each Fourier mode as a sinusoid, uses equation (43) to quantify the effective roughness associated with each sinusoid, and then sums the contributions of each sinusoid to determine the total effective z_0 value, fully taking into account microtopographic variations across a wide range of scales.

Within the implementation of the DFT in the IDL programming language, the amplitude of each Fourier mode is equal to 2 times the amplitude of the complex Fourier coefficient, i.e. $a_n = 2|f_n|$, and the maximum slope is given by $S_n = 2\pi ka$, where k is the natural wavenumber. As such, the generalization of equation (4) to multiscale topography as quantified using the DFT is

$$z_0 = z_{0g} + \sum_{n=1}^{N} z_{0n} \quad \text{where} \quad z_{0n} = \frac{2c_4|f_n|}{1 + \left(c_2/|4\pi kf_n|\right)^{c_3}} . \tag{5}$$

(4)

where c_4 is a unitless coefficient analogous to c_1 but with a potentially different value, and k is the natural wavenumber defined as the inverse of the wavelength. We verified that equation (5̶4) returns the same value of z_0 as predicted by equation (4̶3) for the case of a sinusoidal bed if $c_4 = c_1$. We also verified that the z_0 values predicted by equation (5̶4) were independent of the total number of data points and the sampling interval of the input data (provided that the dominant scales of roughness were represented and resolved). The best-fit value of c_4 was obtained by a brute-forced trial-and-error minimization of the least-squared difference between the predictions of equation (5̶4) and the mean z_0 values measured at the ten sites.

An alternative approach to equation (4) that is easier to apply and does not rely on the Fourier transform is

$$z_0 = z_{0g} + c_5 H_{\text{RMSE}} S_{\text{av}}^{c_6} , \tag{5}$$

where c_5 and c_6 are unitless coefficients.

3. Results

3.1. TLS surveying

Figure 4 presents color maps of the topography of the roughest and smoothest sites at each playa. Table 1 presents summary statistics for the ten sites, including the topographic metrics H_{RMSE} and S_{av}.

Figure 5 plots the average amplitude spectrum of all 1D topographic transects for each site. These spectra demonstrate that significant topographic variability exists at all spatial scales of measurement, i.e. from 0.02-10 m (note that two samples are required for Fourier analysis, hence the smallest wavelength captured in our analysis is $2\Delta x$ or 0.02 m). A surface with a single scale of roughness, such as wind ripples, would have power concentrated at a narrow range of wavelengths, unlike the "broadband" spectra of Figure 5. Also, note that the different shapes of the spectra reflect the different spatial scales that dominate topographic variability at each site. At Willcox Playa, for example, the largest roughness elements occur at horizontal spatial scales ~1-3 m (Figs. 4D&4E). As a result, the power spectra for the Willcox sites exhibit a "bend" at wavelengths of approximately 1-3 m, indicating that the amplitude of the microtopography drops off substantially at wavenumbers larger than 0.3-1, i.e. wavelengths smaller than 1-3 m. A similar bend occurs in the Lordsburg rough site but at a higher wavenumber corresponding to a wavelength of ~0.03-0.1 m. The color map of the Lordsburg rough site is consistent with this, i.e. it shows a "dimpled" surface with large roughness elements ~0.03-0.1 m in size.

3.2. Measurement and analyses of wind profiles

Figure 6 plots the relationship between the average wind velocity (normalized to the value measured at 2.8 m above the ground) and the natural logarithm of height above the ground for all sites. The data have been normalized to emphasize how z_0 and deviations from equation (1) vary among the sites (neither of which depend on absolute velocity values). Note that the

three Death Valley sites have been shifted to the left along the x axis by 0.1 m s^{-1} to help differentiate the plots.

The law of the wall predicts a constant slope when u is plotted ~~versus ln z.~~vs. ln z. When the velocities are normalized as in Figure 6, a steeper slope corresponds to a smaller z0 value. The slopes of the lines in Figure 6 systematically decrease (hence mean z_0 values increase) from the smoothest playa (Lordsburg) to the roughest (Death Valley). Within each playa, the slopes also systematically decrease from relatively smooth sites to rough sites (Table 1). The plots in Figure 6 suggest that the lowest two sensors (located 0.01 and 0.035 m above the ground) at the Death Valley sites and the rough Soda Lake site reside within the roughness sublayer and hence should not be used to obtain z_0 values via least-squares fitting of data to equation (1). The same is true for the lowest sensor at the four smoother sites (all but the two smoothest sites at Lordsburg Playa).

Histograms of z_0 values measured at each site are presented in Figures 7A&7C. As noted in section 2.2, a z_0 value was calculated for each 12 s interval for which a least squares fit of u to ln z yielded a R^2 value of greater than 0.95. Figure 7 shows that z_0 values are approximately lognormally distributed. Sites that have higher-amplitude microtopographic variations at the 0.01 m scale (as measured by the average amplitude spectra in Figure 5) have higher z_0 values. Aside from measurement error/uncertainty, there are two reasons for variance in measured z_0 values. The first is the fluctuating nature of turbulence itself. This source of variance can be reduced by averaging the wind velocities over longer time intervals before fitting to equation (1). The second source of variance comes from moving the hotwire sensors to different locations around each site, thereby "sampling" different patches of microtopography. We found this second source to be the dominant source of variation based on the fact that z_0 values exhibit much greater

variability over time scales of ~1 h, i.e. the time scale over which the hot-wire sensors were moved around the landscape.

Values of mean z_0 for each site have a power-law dependence on H_{RMSE} (Fig. 8A), i.e.

$$z_0 = cH_{RMSE}^{b} \tag{65}$$

where $c = 6 \pm 1$ m^{-1} and $b = 2.0 \pm 0.1$ and the uncertainty values represent 1σ standard deviations. Equation (65) is broadly consistent with the results of Nield et al. (2014) (equation (2)). The value of the exponent b we obtained is slightly higher than that of Nield et al. (2014), but such a difference is not unexpected considering that we are studying different playas.

There are several limitations with using H_{RMSE} as the sole or primary predictive variable for z_0. First, a nonlinear relationship between z_0 and H_{RMSE} yields unrealistic values when applied outside the range of spatial scales considered here and in Nield et al. (2014). For example, using equation (65) with H_{RMSE} values in the range of predicts z_0 values in the range of 6-54 m, i.e. values larger than any value ever measured. Playa surfaces rarely, if ever, have H_{RMSE} values of 1-3 m, but many other landscapes (e.g. alluvial fans) do. Since the goal of this work is to use playas as model landscapes for understanding the multi-scale controls on z_0 above landscapes in general (not playas specifically), it is necessary for any empirical equation to predict reasonable results for a broad range of landscape types and a range of spatial scales beyond the specific range considered in the model calibration. Second, H_{RMSE} values are problematic to use as the sole or dominant variable for use in predicting z_0 values because they contain no information about terrain slope. A topographic transect with a point spacing of 0.01 m can be "stretched" to obtain any slope value, with importance consequences for flow separation and z_0 values.

Figure 8B plots the relationship between mean z_0 and S_{av}, the mean slope computed between adjacent points at the 0.01 m scale, for the ten study sites. This figure documents a

systematic nonlinear relationship between z_0 and S_{av}, suggesting that the nonlinearity between z_0

and H_{RMSE} in equation (6) may reflect a dependence of z_0 on S_{av} in addition to a dependence of z_0

on H_{RMSE}. This hypothesis is consistent with Figure 8C, which demonstrates that H_{RMSE} values

are highly correlated with S_{av} values, i.e. that, in the playa surfaces we studied, playas with larger

microtopographic amplitudes are systematically steeper. We would not expect such a correlation

between amplitude and steepness to apply to all landform types because, as microtopography

transitions into mesotopography and H_{RMSE} increase from 0.1 to 1 and higher, slope gradients do

not continually steepen without bound. If our goal is to understand the controls on z_0 values in

landscapes generally, the data in Figure 8 suggests that it is necessary to quantify the separate

controls of amplitude and slope on z_0 values. This was the purpose of the CFD modeling

described in the next section.

3.3. Computational fluid dynamics

~~Figure 9~~ To demonstrate the suitability of PHOENICS for modeling atmospheric

boundary-layer flows and to establish that the effective roughness length depends on the

microtopographic variability at multiple scales, we performed a numerical experiment using the

central microtopographic profile measured at the Soda Lake smooth site as input (plotted in Fig.

9A). We measured a mean z_0 value of 4.6 mm from velocity profiles at this site. Figure 9B

presents the velocity profiles predicted by the PHOENICS model for 2D flow over the profile,

following the procedures detailed in the Methods section. PHOENICS predicts an effective

roughness length of 2.4 mm based on a least-squares fit of the velocity to the logarithms of

distance above the ground from a height equal to twice the height of the dominant roughness

elements to the top of the model domain. As such, the PHOENICS model predicts a z_0 value

similar to the value we measured in the field (relative to the four order-of-magnitude variation in z_0 values we measured across the study sites).

To demonstrate that the z_0 value depends on microtopographic variability at multiple scales, we filtered the Soda Lake smooth profile diffusively to remove some of the small-scale (high-wavenumber) variability while maintaining the large-scale variability (i.e. the root-mean-squared variability of the filtered and unfiltered profiles is identical). Figure 9 plots the original profile, the filtered profile, and their amplitude and z_{0n} spectra. The z_0 values for the unfiltered and filtered cases are 2.4 mm and 0.15 mm, respectively, based on fitting the velocity profiles predicted by PHOENICS. That is, the filtered profile has a z_0 value more than an order of magnitude smaller than the original profile despite the fact that the amplitude of the large-scale microtopographic variations is the same as the original profile. Equation (3) predicts 2.8 mm and 0.25 mm, respectively, for the z_0 values. The z_0 value decreases in the filtered case because steep slopes that trigger flow separation are significantly reduced at a wide range of scales by filtering, lowering the z_0 value.

The results of this numerical experiment demonstrate that z_0 values depend on variability microtopographic variability at multiple scales. There is also a general theoretical argument that supports this conclusion. If one accepts that both the amplitude and slope of the microtopography influence the effective roughness length (which we will demonstrate below for the case of a sinusoid), it follows that there is no single Fourier mode that controls the effective roughness length, unless the topography is a perfect sinusoid. This is because the slope is a high-pass filter of the topography (i.e. the slope is proportional to $k*a_n$ where an is the Fourier coefficient) and hence is more sensitive to high-wavenumber components of the topography than the amplitude is.

Figure 10 presents color maps that illustrate the output of the CFD model for an example case ($a = 0.05$ m and $S = 0.79$ m/m). Figure ~~9A~~10A, which shows a color map of the turbulent kinetic energy, illustrates the growth of the internal boundary layer with increasing distance from the upwind boundary of the domain as the input velocity profile interacts with and adjusts to the presence of the microtopography. Figures ~~9B&9C~~10B&10C zoom in on the flow and illustrate the zones of flow separation that occur in this example. These figures also illustrate the ~~terriain~~terrain-following and logarithmically spaced nature of the computational grid in the vertical direction.

Figure ~~10~~11 plots the z_0 values computed from an analysis of the CFD-predicted wind profiles over sinusoidal topography for two different values of the sine-wave amplitude ($a = 0.05$ m and 0.1 m) and for a range of values of the maximum slope S from approximately 0.001 to 2.0. For maximum slope values less than approximately 0.004, the z_0 value is equal to z_{0g}, as we would expect (the topography is effectively flat). As the slope of the microtopography increases, the wind field is increasingly perturbed by the roughness of the terrain. Eventually, flow separation is triggered and flow recirculation zones are created in the wakes of each bedform, further increasing z_0 values. For very steep slopes, i.e. $S \sim 0.4$-1, z_0 values still increase with increasing slope but at a slower rate than for gentler slopes since the flow as already separated and additional steepening has only a modest effect on the spatial extent of flow separation and z_0 values. The nonlinear dependence of z_0 on S is well fit by a sigmoidal relationship of the form given by equation (4). Best-fit values are $c_1 = 0.1$, $c_2 = 0.4$, and $c_3 = 2.0$.

3.4. Fourier analysis of topography and a multi-scale approach to quantifying z_0 and the z_{0n} spectrum

Using a brute-force minimization of the squared difference between the mean measured values of z_0 and the values predicted by equation (5) for all study sites, we found the optimal value of c_4 to be 1.5. Figure ~~11~~12 plots z_{0n} values computed by equation (5) as a function of the natural wavenumber, k. The sum of all the z_{0n} values is the predicted value of z_0 for each surface. There is also value, however, in examining the dependence of z_{0n} on the wavenumber. The plot in Figure ~~11~~12 shows which spatial scales are most dominant in controlling the value of z_0 for a given landscape (see arrows in Fig. ~~11~~12). On Lordsburg Playa, the only spatial scales that have non-negligible slope gradients are those at 0.01-0.3 m. At the rougher sites, the dominant roughness elements are found at different scales, from 0.1-1 m (Soda Lake) to 1-10 m (Willcox Playa) to 0.3-3 m (Death Valley). This plot also shows that in some cases there is one dominant scale of roughness elements (e.g. Soda Lake and Death Valley) while in others there are two or more scales that are equally dominant (e.g. Willcox Playa).

Figure ~~12~~13 plots the z_0 values predicted by equation (~~5~~4) versus the mean measured values for the ten study sites. Note that there appears to be only nine points plotted in Figure ~~12~~13 because two of the points (for Lordsburg smooth and Lordsburg intermediate) are nearly indistinguishable. The correlation between the logarithms of the predicted and measured mean z_0 values is quite good ($R^2 = 0.991$). Equation (~~5~~4) is capable of predicting z_0 values to 50% accuracy, on average, across a four order-of-magnitude range.

An alternative approach is to use the values of H_{RMSE} and S_{av} to estimate z_0 using equation (5). We found $c_5 = 16$ and $c_6 = 2.0$ to yield the highest R^2 value (0.978). Equation (5) is thus a useful formula with an advantage of simplicity, but it is somewhat inferior to the multi-scale analysis of equation (4) based on its lower R^2 value.

4. Discussion and Conclusions

The values of c_3 and c_2 respectively reflect the magnitude of the nonlinear increase in z_0 values as slope increases and the slope value where back-pressure effects begin to limit the rate of increase in z_0 with increasing slope. The ~~value~~values of c_3 and c_6 (2.0) reflects a square relationship between roughness length and the maximum slope of microtopographic variations at a given scale, which is broadly consistent with the nonlinear relationship between z_0 values and maximum slope in the model of Jacobs (1989) (note, however, that the ~~Jacobs'~~Jacobs (1989) model ~~only~~ applies only to gentle slopes that do not trigger flow separation). The value of c_2 (0.4 or 24°) is similar to the critical/maximum angle of attack of typical aerofoils (Bertin and Cummings, 2013). Critical angles of attack represent the maximum steepness possible before the drag effects become greater than lift due to excessive pressure drag and the associated lee-side flow separation. Similarly, the value of c_2 represents the maximum slope of the microtopography in which an increase in slope leads to a nonlinear increase in z_0 values. Above this slope value, z_0 values increase more modestly with increasing slope because flow separation already occurs over a significant portion over the surface.

~~The approach of this paper is limited in that it applies the superposition principle to a problem for which it cannot apply precisely (superposition applies only to linear systems). The limited applicability of the superposition principle to this problem may be one reason why the value of the value of c_4 is larger than c_1. If superposition were to apply exactly, we would expect equation (5) to be an exact Fourier-based implementation of equation (4) with the same values of the coefficients. Instead, we found that the best-fit value of c_4 is approximately fifteen times larger than c_1. The high correlation coefficient between the model and data (obtained with just one free parameter) suggests that our approach is reasonable, but the difference between the~~

~~values of c_1 (the mono-scale case) and c_4 (the multi-scale case) points to the limited applicability~~ ~~of the superposition principle in this case. Despite this limitation, we believe that our approach is~~ ~~a reasonable first step towards quantifying the multi-scale controls on z_0 values until a more~~ ~~comprehensive and fully nonlinear approach is found.~~ The CFD model results demonstrate that equation (3) works well for a single sinusoid, while equation (4) works well for real-world cases that can be represented as a superposition of many (i.e., $N \gg 1$) sinusoids. The fact that the value of c_4 is larger than c_1 indicates that there is no seamless transition between equation (3) and equation (4) as the topography changes from the idealized case of a single sinusoid to the case of many superposed sinusoids. That is, neither formula works well for the case of a small number of superposed sinusoids. The absence of such a seamless transition could be a result of applying the superposition principle to a nonlinear problem (boundary layer turbulence) for which it cannot apply precisely. In addition, experimental studies demonstrate that flow separation (which influences z_0) is a function of both the slope and the curvature of the bed (Simpson, 1989; Lamballais et al., 2010). Equations (3) and (4) do not utilize curvature, hence neither equation can be the basis of a perfect method for predicting z_0. It is likely that the only way to precisely estimate z_0 is to compute the actual flow field over the topography using a CFD model. Any other approach will likely involve some type of approximation. We propose that equation (4), while imperfect, yields a good approximation for z_0 values in real-world terrain (i.e. those with many Fourier coefficients contributing to z_0), based on the R^2 value of 0.991 we obtained. Equation (5) provides an alternative for users who prefer its simplicity. Equation (5) is not accurate for all possible S_{av} values, since z_0 cannot increase without bound as S_{av} increases. As such, equation (5) should only be considered applicable for microtopography with S_{av} values less than approximately 0.15.

We developed and tested a new empirical formula for the roughness length, z_0, of the fully rough form of the law of the wall that uses the amplitude and slope of microtopographic variations across multiple scales within a discrete-Fourier-transform-based approach. A sigmoidal relationship between z_0 and the amplitude and slope of sinusoidal topography developed from CFD model results was used to quantify the effects of each scale of microtopography on z_0. The model was developed and tested using approximately sixty thousand z_0 values from the southwestern U.S. obtained over 2.5 orders of magnitude in distance above the bed. The proposed method is capable of predicting z_0 values to 50% accuracy, on average, across a four order-of-magnitude range. This approach adds to our understanding of and ability to predict the characteristics of turbulent boundary flows over landscapes with multi-scale roughness.

Data Availability

DEMS of each of the study sites (relative elevation in m) and mean wind velocities (in m s^{-1}) measured at seven heights above the ground at 12-s intervals are available as Supplementary files.

References

Arya, S. P. S.: A drag partition theory for determining the large-scale roughness parameter and wind stress on the Arctic pack ice, J. Geophys. Res., 80, 3447-3454, 1975.

Bagnold, R. A.: The movement of desert sand, Proc. R. Soc. London, Set. A, 157, 594–620, 1938.

Bauer B.O., Sherman, D.J., and Wolcott J.F.: Sources of uncertainty in shear stress and roughness length estimates derived from velocity profiles, Prof. Geogr., 44, 453–464, 1992.

Bertin, J. J., and Cummings, R. M.: Aerodynamics for Engineers, sixth edition, Prentice-Hall, New York, 2013, 832 p.

Brown, O. W., and Hugenholz, C. H.: Quantifying the effects of terrestrial laser scanner settings and survey configuration on land surface roughness measurement, Geosphere, 9(2), 367–377, doi:10.1130/GES00809.1, 2013.

Counehan, J.: Wind tunnel determination of the roughness length as a function of the fetch and the roughness density of three-dimensional roughness elements, Atmos. Environ., 5(8), 637–642, doi:10.1016/0004-6981(71)90120-X, 1971

Dong, Z., Wang, X., Zhao, A., Liu, L., and Liu, X.: Aerodynamic roughness of fixed sandy beds, J. Geophys. Res., 106(6), 11,001-11,011, 2001.

Elliot, W. P.: The growth of the atmospheric internal boundary layer, EOS Trans. AGU, 38, 1048, 1958.

Gomez, B., and Church, M.: An assessment of bed load sediment transport formulae for gravel bed rivers, Water Resour. Res., 25, 1161–1186, 1989.

Hodge, R. A.: Using simulated Terrestrial Laser Scanning to analyse errors in high-resolution scan data of irregular surfaces, ISPRS J. Photogramm. Remote Sens., 65 (2), 227–240, 2010.

Jackson, P. S.: On the displacement height in the logarithmic velocity profile, Journal of Fluid Mechanics, 111, 15–25, 1981.

Jacobs, S. L.: Effective roughness length for turbulent flow over a wavy surface, J. Phys. Oceanogr., 19, 998–1010, 1989.

Kean, J. W., and Smith, J. D.: Form drag in rivers due to small-scale natural topographic features: 1. Regular sequences, J. Geophys. Res., 111, F04009, doi:10.1029/2006JF000467, 2006a.

Kean, J. W., and Smith, J. D.: Form drag in rivers due to small-scale natural topographic features: 2. Irregular sequences, J. Geophys. Res., 111, F04010, doi:10.1029/2006JF000490, 2006b.

Lamballais, E., Silvestrini, J., and Laizet, S.: Direct numerical simulation of flow separation behind a rounded leading edge: Study of curvature effects, Inter. J. Heat Fluid Flow, 31, 295-306, doi:10.1016/j.ijheatfluidflow.2009.12.007, 2010.

Lettau, H.: Note on Aerodynamic Roughness-Parameter Estimation on the Basis of Roughness-Element Description, J. Appl. Meteorol., 8, 828–832, doi:10.1175/1520-0450(1969)008<0828:NOARPE>2.0.CO;2, 1969.

Ludwig, J. C.: PHOENICS-VR Reference Guide, CHAM Ltd., London, U.K., digital document available online at http://www.cham.co.uk/documentation/tr326.pdf, 2011.

Nakato, T.: Tests of selected sediment-transport formulas, J. Hydraulic Eng., 116, 362–379, 1990.

Namikas, S. L., Bauer, B. O., and Sherman, D. J.: Influence of averaging interval on shear velocity estimates for aeolian transport modeling, Geomorphology, 53(3-4), 235–246, 2003.

Nield, J. M., et al.: Estimating aerodynamic roughness over complex surface terrain, J. Geophys. Res. Atmos., 118, 12,948–12,961, doi:10.1002/2013JD020632, 2014.

Patankar, S. V., and Spalding, D. B.: A calculation procedure for heat, mass and momentum transfer in three-dimensional parabolic flows, Inter. J. Heat Mass Transfer, 15, 1782–1806, doi:10.1016/0017-9310(72)90054-3, 1972.

Prigent, C., Tegen, I., Aires, F., Marticorena, B., and Zribi, M.: Estimation of the aerodynamic roughness length in arid and semi-arid regions over the globe with the ERS scatterometer, J. Geophys. Res., 110, D09205, doi:10.1029/2004JD005370, 2005.

Raupach, M. R.: Drag and drag partition on rough surfaces, Boundary Layer Meteorol., 60(4), 375–395, 1992.

Raupach, M. R.: Simplified expressions for vegetation roughness length and zero-plane displacement as functions of canopy height and area index, Boundary-Layer Meteor., 71(1-2), 211–216, doi:10.1007/BF00709229, 1994.

Sherman, D. J., and Farrell, E. J.: Aerodynamic roughness length over movable beds: Comparison of wind tunnel and field data, J. Geophys. Res., 113, F02S08, doi:10.1029/2007JF000784, 2008.

Simpson, R. L.: Turbulent boundary-layer separation, Ann. Rev. Fluid Mech., 21, 205–234, 1989.

Smigelski, J. R.: Water level dynamics of the North American Great Lakes: Nonlinear scaling and fractional Bode analysis of a self-affine time series, unpublished Ph.D. dissertation, Wright State University, 890 p., 2013.

Smith, J. D., and McLean, S. R.: Spatially averaged flow over a wavy surface, J. Geophys. Res., 82(12), 1735–1746, 1977.

Spalding, D. B.: Mathematical Modelling of Fluid-Mechanics, Heat-Transfer and Chemical-Reaction Processes, CFDU Report HTS/80/1, Imperial College, London, 1980.

Taylor, P. A., Sykes, R. I., and Mason. P. J.: On the parameterization of drag over small-scale topography in neutrally-stratified boundary-layer flow, Bound. Layer Meteor., 48(4), 409–422, 1989.

Yakhot, V., and Orszag, S. A.: Renormalization group analysis of turbulence, J. Sci. Comput., 1, 3–51, doi:10.1007/BF01061452, 1986.

Yakhot, V., Orszag, S. A., Thangam, S., Gatski, T. B., and Speziale, C. G.: Development of turbulence models for shear flows by a double expansion technique: Phys. Fluids A, 4(7), doi: 10.1063/1.858424, 1992.

Table 1. Study site locations ~~and,~~ attributes~~.~~, and predictions of equations (4) and (5).

Name	Latitude (° N)	Longitude (° W)	# profiles	H_{RMSE} (mm)	S_{av}	mean z_0 (mm)	pred. z_0 Eqn. (4) (mm)	pred. z_0 Eqn. (5) (mm)
Death V. rough	36.34449	116.86338	8036	34	0.144	23	34	11
Death V. interm.	36.34466	116.86321	10922	36	0.142	16	26	12
Death V. smooth	36.34485	116.86307	9457	26	0.122	6.3	10	6.2
Soda Lake rough	35.15845	116.10413	10838	14	0.159	7.6	4.1	5.7
Soda Lake smooth	35.15852	116.10352	7134	11	0.154	4.6	2.8	4.2
Willcox rough	32.16882	109.88889	6404	6.6	0.056	0.26	0.22	0.33
Willcox smooth	32.14869	109.90317	2403	4.8	0.076	0.16	0.14	0.44
Lordsburg rough	32.28137	108.88378	1883	1.3	0.032	0.047	0.020	0.021
Lordsburg interm.	32.28105	108.88400	2569	0.72	0.017	0.002	0.0026	0.0033
Lordburg smooth	32.28097	108.88459	203	0.55	0.017	0.002	0.0025	0.0025

Figure 1. Plots of synthetic (top) and real (middle and bottom) topographic transects illustrating the multi-scale nature of topography using natural playa surfaces as examples.

Figure 2. Aerial images of the study sites.

Figure 3. Photographs of the equipment used for measuring wind profiles. (A) Mast holding 4 hot-wire anemometers (left) and four cup anemometers (right, note that only the lowest 3 are visible) at the Animas intermediate study site. (B) Close-up photograph of the hot-wire sensors at the Soda Lake smooth site. For scale, note that the top hot-wire sensor is located 0.16 m above the surface in both photographs.

Figure 4. Color maps of TLS-derived DEMs of eight of the ten study sites. (A) Death Valley rough, (B) Death Valley smooth, (C) Soda Lake rough, (D) Soda Lake smooth, (E) Willcox rough, (F) Willcox smooth, (G) Lordsburg rough, (H) Lordsburg smooth. Note the differing color scales between (A)&(B) and (C)&(D).

Figure 5. Plots of the average amplitude spectrum, A, of 1D transects of the microtopography of each site as a function of the natural wavenumber, k. The colors red, green, blue, and black are used to represent the Death Valley, Soda Lake, Willcox, and Lordsburg sites, respectively. Thicker curves represent rougher sites within each playa.

Figure 6. Plots of mean wind velocity (normalized by the velocity measured at the highest sensor, located 2.8 m above the ground) (x axis) as a function of the natural logarithm of height above the ground (y axis). The colors red, green, blue, and black are used to represent the Death Valley, Soda Lake, Willcox, and Lordsburg sites, respectively. Within each playa, thicker lines are used to represent the rougher sites. Open circles indicate stations located within the roughness sublayer. These sensors were not used to calculate z_0.

Figure 7. (A)-(B) Normalized histograms of z_0 values measured at each site and (C)-(D) probability distributions for each site, assuming z_0 values are log-normally distributed.

Figure 8. Plots of mean z_0 at each site versus (A) H_{RMSE} and (B) S_{av}. (C) Plot of H_{RMSE} vs. S_{av}.

Figure 9. Demonstration of the dependence of z_0 values on the multi-scale nature of microtopography. (A) Plot of a profile through the Soda Lake smooth site (thin curve). Also shown is the same plot with diffusive smoothing (thicker curve). Smoothing maintains the amplitude of microtopographic variations at large spatial scales (i.e. the amplitude spectrum is unchanged at large scales) but removes some of the small-scale (high-wavenumber) variability. (B) Plots of the mean velocity profiles predicted by PHOENICS over the original and filtered

profile. (C) Amplitude spectra of the two plots in (A). (D) Contributions of each Fourier mode to the z_0 values for the two plots in (A).

Figure 10. Illustrations of the output of the PHEONICS CFD model for the example case (with amplitude $a = 0.05$ m and maximum slope $S = 0.79$ m/m) of flow over a sinusoidal bed. (A) Color map of turbulent kinetic energy, *KE*. This map illustrates the growth of the internal boundary layer triggered by the effective roughness change as the input velocity profile (characterized by a grain-scale roughness z_{0g}) interacts with and adjusts to the microtopography. The color vector maps in (B) and (C) illustrate the zones of flow recirculation that occur in the lee side of each bedform.

Figure ~~10~~11. Plot of the z_0 value predicted by the PHOENICS CFD model for flow over sinusoidal terrain with two values of the amplitude, *a*, and a wide range of values of the maximum slope values, *S*. Also shown are predictions of equation (~~4~~3) for the best-fit parameter values.

Figure ~~11~~12. Plots of the contribution of each Fourier mode to the effective roughness length, z_{0n}, as a function of *k*. Arrows point to the range of wavenumbers that contribute most to z_0.

Figure ~~12~~13. Plot of mean measured z_0 values versus predicted values (~~from equation (5~~using Eqn. (4))) for the ten study sites. Error bars denote 1σ variations in the measured z_0 values.